



Bachelor's Thesis  
Theoretical Physics

## **Role of surface plasmons in light emitting diode structures**

Teemu Laakso  
2013

Instructors: Dr. Toufik Sadi  
Dr. Jani Oksanen  
Examiner: Dr. Antti Kuronen

UNIVERSITY OF HELSINKI  
DEPARTMENT OF PHYSICS

PL 64 Gustaf Hallströmin katu 2  
00014 Helsingin yliopisto

## **Abstract**

The goal of this report is to provide an initial theoretical framework for analyzing and investigating the coupling of light emission from an InGaN quantum well to surface plasmons (SPs). The research is motivated by the need to explain the source of interference patterns observed in measurements performed by the Optoelectronics Group at Micronova research center, Aalto Yliopisto, led by Markku Sopanen. Specifically, the features introduced by thin periodic silver grating in planar layered media are studied through a combination of analytical solutions of Maxwell's equations and the transfer matrix method. The methods are used to determine the optical properties of the structures, including the dispersion relations of the bound modes, the electric field profiles and the reflectivity spectrum of the system. The effect of silver grating is included by folding the wavevectors as an approximation of the structural effects. Results produced by the developed model showed good agreement with experimental data. Analysis of theoretical results allowed the identification of the source for the observed interference patterns; the mixing of the plasmonic and guided modes. The model also provided further insight in the optimization of layer composition and dimensions to maximize the coupling of the plasmonic modes with the light-emitting quantum well.

# Contents

<b>1</b>	<b>Introduction</b>	<b>4</b>
<b>2</b>	<b>Theoretical Background</b>	<b>5</b>
2.1	Electromagnetic Properties of Matter . . . . .	5
2.1.1	Maxwell's Equations . . . . .	5
2.1.2	Boundary Conditions . . . . .	6
2.1.3	Drude Model . . . . .	7
2.2	Surface Plasmons in Simple Geometries . . . . .	8
2.2.1	Surface Plasmons at a Single Interface . . . . .	8
2.2.2	Skin Depth . . . . .	10
2.2.3	Surface Plasmons in Thin Films . . . . .	11
2.3	The Effect of a Grating . . . . .	13
<b>3</b>	<b>Computational Methods</b>	<b>14</b>
3.1	Transfer Matrix Method . . . . .	14
3.1.1	Field Propagation and the Propagation Matrix . . . . .	14
3.1.2	Interface of Two Semi-Infinite Materials . . . . .	15
3.2	The General Form . . . . .	16
3.2.1	Reflectivity and Transmissivity . . . . .	16
3.2.2	Electric Field Profile . . . . .	17
3.2.3	Bound Modes . . . . .	17
<b>4</b>	<b>Simulation Results and the Experimental Setup</b>	<b>19</b>
4.1	The Experimental Setup . . . . .	19
4.2	Modeled Structure . . . . .	19
4.3	Analysis of the Structure . . . . .	19
4.3.1	Reflectivity . . . . .	20
4.3.2	Bound Modes . . . . .	21
4.3.3	Effects of the Grating . . . . .	24
<b>5</b>	<b>Conclusions</b>	<b>26</b>
	<b>Appendices</b>	<b>27</b>

# 1 Introduction

From the pioneering work of Richie [?] in the 1950s up to the late 1990s, surface plasmons (SPs) were largely considered a topic of academic interest. This was due to the fact that the technology of the time could not utilize surface plasmons commercially. However, a shift in the interest has been seen after many technical advances in characterization and processing of metal surfaces leading to better understanding of the potential applications of SPs. The first major discovery was the identification of the role played by surface plasmons in the phenomenon of extraordinary transmission of light (EOT) [?]. The experiment by Ebbensen *et al.* suggested that surface plasmons showed intriguing properties at the nanometer scale. Even though no specific idea utilizing surface plasmons has seen a commercial breakthrough, small steps are constantly taken. For example, light absorption technology in solar cells has seen an increase in the total absorption through the use of plasmons [?]. Additionally, the possibilities for the next generation photonic devices are numerous; they vary from enhancement of light emitting materials [?] to plasmonic lasers [?], and even to sub-wavelength microscopy [?].

This thesis introduces an initial theoretical framework for describing an experiment performed by the department of Micro and Nanosciences at Aalto University, and the Laboratory of Condensed Matter Physics and Nanostructures at the University of Claude Bernard in Lyon. The purpose of the experiment is to study the coupling between a quantum well and the surface plasmons of a metal. In the experiment, a thin periodic metal grating is placed near a quantum well. It is predicted that this should change the distribution of states into which the quantum well excites photons, allowing strong coupling to the plasmons on the surface of the metal. If the metal is thin enough, the surface plasmons on the top and bottom interfaces may further couple to each other. With proper optimization of the shape of the metal, the surface plasmons could also be coupled to the free optical modes. Ideally, this increases the total luminescence and energy efficiency of the light emission.

The aim of this thesis is to create an introductory model for a layered planar system containing a periodic metal grating. The primary goal is to study the basic optical properties of such system, and to compare them to the experimental results, as well as to explain the main features of the physical phenomena taking place between a quantum well and the metal grid. It is worth noting that the model was created as the experiments were ongoing, and the preliminary results of the study were useful in guiding the experiment.

The structure of the thesis is as follows. In chapter 2, the basic electromagnetic theory leading to surface plasmons is discussed. This will include an introduction to the properties of surface plasmons in planar structures. In chapter 3, the use of the transfer matrix method in studying the properties of parallel planar structures is described. In chapter 4 the model is applied to stimulate the structure used in experiments. The reflective properties of the structure are discussed and compared to the experimental results. Chapter 5 summarizes the important aspects of this work, and discusses future prospects of the theoretical work.

## 2 Theoretical Background

This section will introduce the basic theoretical framework for modeling surface plasmons; a short discussion will be presented for the most important SP properties. Surface plasmons will be considered from a classical point of view, i.e. microscopic charge distributions and nonlocal responses are ignored. A more detailed discussion on the properties of surface plasmons is given by Pitarke [?].

### 2.1 Electromagnetic Properties of Matter

#### 2.1.1 Maxwell's Equations

The basic properties of surface plasmons are described by Maxwell's equations, which describe the evolution of electric and magnetic fields in a given structure. They are defined by:

$$\nabla \times \mathbf{E} = -\frac{\partial \mathbf{B}}{\partial t}, \quad (1a)$$

$$\nabla \times \mathbf{H} = \frac{\partial \mathbf{D}}{\partial t} + \mathbf{J}, \quad (1b)$$

$$\nabla \cdot \mathbf{D} = \rho, \quad (1c)$$

$$\nabla \cdot \mathbf{B} = 0, \quad (1d)$$

where  $\mathbf{E}$  is the electric field,  $\mathbf{D}$  is the electric displacement field,  $\mathbf{H}$  is the magnetic field,  $\mathbf{B}$  is the magnetic flux density,  $\rho$  is charge density, and  $\mathbf{J}$  is the current density. The field strengths are related to the respective fluxes by the constitutive equations:

$$\mathbf{D} = \varepsilon \mathbf{E}, \quad (2a)$$

$$\mathbf{B} = \mu \mathbf{H}, \quad (2b)$$

where  $\varepsilon$  is the permittivity and  $\mu$  the permeability of the material. All materials in question are assumed to be non-magnetic and isotropic. This means that the dielectric functions will only be a function of frequency ( $\varepsilon = \varepsilon(\omega)$ ), and that the materials are non-responsive to magnetic fields ( $\mu = \mu_0 = 4\pi \times 10^{-7} \frac{\text{N}}{\text{A}^2}$ ). Combining Maxwell's equations assuming that there are no free sources ( $\rho = 0$ ) or currents ( $\mathbf{J} = 0$ ) results in the wave equation for the electric and magnetic fields, given by

$$\nabla^2 \mathbf{E} - \mu \varepsilon \frac{\partial^2 \mathbf{E}}{\partial t^2} = 0, \quad (3a)$$

$$\nabla^2 \mathbf{H} - \mu \varepsilon \frac{\partial^2 \mathbf{H}}{\partial t^2} = 0. \quad (3b)$$

One solution to the wave equation is the planewave. Thus, the electric and magnetic fields can be represented in the Cartesian coordinate system as planewaves

$$\mathbf{E}_{\pm} = \begin{pmatrix} E_x \\ E_y \\ E_z \end{pmatrix} e^{i(\pm \mathbf{k} \cdot \mathbf{r} - \omega t)}, \quad (4a)$$

$$\mathbf{H}_{\pm} = \begin{pmatrix} H_x \\ H_y \\ H_z \end{pmatrix} e^{i(\pm \mathbf{k} \cdot \mathbf{r} - \omega t)}, \quad (4b)$$

where  $E_{x,y,z}$  and  $H_{x,y,z}$  are field components determining the field polarization in  $x$ ,  $y$ , and  $z$  directions respectively,  $\omega$  is the angular frequency of the wave,  $\mathbf{k}$  is the wavevector, and  $i$  is the imaginary unit ( $i^2 = -1$ ). The wavevector further satisfies the condition:  $k^2 = \mu\epsilon\omega^2$ . The degrees of freedom in the solution allow representing the solutions independently as two linear solutions: transverse electric (TE, s-polarized) and transverse magnetic polarizations (TM, p-polarized). In this study, the following definitions for the polarizations are used:

$$\mathbf{E}_{\text{TE}} = \begin{pmatrix} 0 \\ E_y \\ 0 \end{pmatrix} e^{i(\pm \mathbf{k} \cdot \mathbf{r} - \omega t)}, \quad \mathbf{H}_{\text{TE}} = \begin{pmatrix} H_x \\ 0 \\ H_z \end{pmatrix} e^{i(\pm \mathbf{k} \cdot \mathbf{r} - \omega t)}, \quad (5a)$$

$$\mathbf{E}_{\text{TM}} = \begin{pmatrix} E_x \\ 0 \\ E_z \end{pmatrix} e^{i(\pm \mathbf{k} \cdot \mathbf{r} - \omega t)}, \quad \mathbf{H}_{\text{TM}} = \begin{pmatrix} 0 \\ H_y \\ 0 \end{pmatrix} e^{i(\pm \mathbf{k} \cdot \mathbf{r} - \omega t)}, \quad (5b)$$

Because this work concerns parallel planar structures, the above definition is utilized when defining the coordinates in the materials. Each planar interface is taken to be in the  $xy$ -plane.

### 2.1.2 Boundary Conditions

The solution to the wave equation Eq. (3) for piecewise homogeneous systems can be constructed from separate planewave solutions Eq. (5) by ensuring that suitable boundary conditions are satisfied. The boundary conditions for electric and magnetic fields are

$$\epsilon_1 E_1^{\perp} - \epsilon_2 E_2^{\perp} = \sigma, \quad (6a)$$

$$\mathbf{E}_1^{\parallel} - \mathbf{E}_2^{\parallel} = 0, \quad (6b)$$

$$B_1^{\perp} - B_2^{\perp} = 0, \quad (7a)$$

$$\frac{1}{\mu_1} \mathbf{B}_1^{\parallel} - \frac{1}{\mu_2} \mathbf{B}_2^{\parallel} = \mathbf{J} \times \mathbf{n}, \quad (7b)$$

where indices 1,2 represent the two materials at the interface,  $E_j^\perp$  and  $\mathbf{E}_j^\parallel$  with  $j = 1, 2$  are the perpendicular and parallel electric field components with respect to the interface, and  $\sigma$  represents the surface charge distribution. Similarly  $B_j^\perp$  and  $\mathbf{B}_j^\parallel$  are the perpendicular and parallel magnetic flux densities components with respect to the interface,  $\mathbf{J}$  represents the surface current, and  $\mathbf{n}$  is the surface normal. Eq. (6b) is especially important, for it states that the component of the electric field that is parallel to the interface remains continuous when moving from one material to the next. When dealing with planewave solutions, this means that the in-plane wavevector is preserved:

$$k_1^\parallel = k_2^\parallel = k_x \quad (8)$$

This condition is one variation of the Snell's law. Notice that in-plane wavevector has been defined parallel to the x-axis. The boundary conditions also give the Fresnel coefficients [?], i.e. the transmissivity and reflectivity of an interface between two semi-infinite materials. The coefficients for TM- (s-) and TE (p) -polarizations are given by:

$$r_{TM} = \frac{k_{iz}\epsilon_t - k_{tz}\epsilon_i}{k_{iz}\epsilon_t + k_{tz}\epsilon_i}, \quad (9a)$$

$$t_{TM} = \frac{2k_{iz}\epsilon_t}{k_{iz}\epsilon_t + k_{tz}\epsilon_i}, \quad (9b)$$

$$r_{TE} = \frac{k_{iz} - k_{tz}}{k_{iz} + k_{tz}}, \quad (10a)$$

$$t_{TE} = \frac{2k_{iz}}{k_{iz} + k_{tz}}, \quad (10b)$$

where  $r_{TM}$ ,  $t_{TM}$ ,  $r_{TE}$  and  $t_{TE}$  represent the reflection and transmission coefficients for electric fields with transverse magnetic and transverse electric polarizations, respectively, and  $k_{iz}$  and  $k_{tz}$  are the perpendicular components of wavevectors of the incident and transmitted waves respectively. These can alternatively be represented as a function of the incidence angle  $\theta$ , but in this work, it is simpler to state them as a function of wavevector components.

### 2.1.3 Drude Model

The Drude model is a classical model proposed to predict the electron response of metals to electric fields. It applies the kinetic theory of gases to a metal, assuming that metals contain free electrons which can be treated in a manner similar to a gas. The model predicts that the average movement of the electrons is proportional to the applied electric field. This allows approximating the permittivity of the metal as [?]

$$\epsilon(\omega) = 1 - \frac{\omega_p^2}{\omega^2 + i\omega\gamma}, \quad (11)$$

where  $\omega$  is the angular frequency of the field,  $\omega_p$  is the metal's plasma frequency, and  $\gamma = \frac{1}{\tau}$ , where  $\tau$

is the relaxation time of the electrons. A further parameterization can be made by replacing the term 1 by a constant  $\epsilon_\infty$ , which approximates the contribution of the bound electrons to the permittivity at the limit  $\omega \rightarrow \infty$ . While this description is phenomenological, it provides an adequate approximation of the optical properties of the layered structures studied in this work.

## 2.2 Surface Plasmons in Simple Geometries

Surface plasmon, or more accurately surface-plasmon-polaritons, are evanescent field solutions to the Maxwell equations confined near an interface with suitable properties [?]. The simplest geometry allowing their existence is the interface between two semi-infinite materials as depicted in Fig. 1. The study of the properties of layered structures will start with a review of the surface plasmons in simple geometries - a single interface between two semi-infinite materials and two interfaces of a film sandwiched between two semi-infinite materials. Since surface plasmons only exist for TM-polarization this section of the work only focuses on TM. Later in the report more complex layered structures are analyzed for both, TE- and TM-polarizations. The values for the dielectric functions used to model materials can be found in appendix A.

### 2.2.1 Surface Plasmons at a Single Interface

In the coordinate system and structure defined in Fig. 1, the waves with transverse magnetic (aka ‘p’) polarization are of the form



Figure 1: The basic structure capable of supporting a surface plasmon: an interface between semi-infinite dielectric and metal. Surface plasmons are evanescent field solutions at the interface of the materials.



$$\begin{aligned}\mathbf{E}_1 &= \begin{pmatrix} E_{1x} \\ 0 \\ E_{1z} \end{pmatrix} e^{i(k_{1x}x - k_{1z}z - \omega t)} \\ \mathbf{H}_1 &= \begin{pmatrix} 0 \\ H_{1y} \\ 0 \end{pmatrix} e^{i(k_{1x}x - k_{1z}z - \omega t)}\end{aligned}, \quad z < 0 \quad (\text{dielectric}), \quad (12a)$$

$$\begin{aligned}\mathbf{E}_m &= \begin{pmatrix} E_{mx} \\ 0 \\ E_{mz} \end{pmatrix} e^{i(k_{mx}x + k_{mz}z - \omega t)} \\ \mathbf{H}_m &= \begin{pmatrix} 0 \\ H_{my} \\ 0 \end{pmatrix} e^{i(k_{mx}x + k_{mz}z - \omega t)}\end{aligned}, \quad z > 0 \quad (\text{metal}), \quad (12b)$$

where  $E_1$  and  $E_m$  are the electric fields in the dielectric and the metal, respectively,  $k_{1z}$  and  $k_{mz}$  are the corresponding wavevector components that are perpendicular to the interface, and  $k_{1x}$  and  $k_{mx}$  are the wavevector components that are parallel to the interface. The boundary conditions [Eq. (6) and (7)] require that the fields parallel to the surface remain continuous:

$$E_{1x} - E_{mx} = 0, \quad (13a)$$

$$H_{1y} - H_{my} = 0. \quad (13b)$$

Eqs. (1b) and (2a) can be used state the electric field components of the solutions in terms of the magnetic field component

$$\frac{k_{1z}}{\varepsilon_1} H_{1y} + \frac{k_{mz}}{\varepsilon_m} H_{my} = 0 \quad (14a)$$

$$H_{1y} - H_{my} = 0, \quad (14b)$$

Solving this system of equations gives the following condition, known as the surface plasmon condition [?]

$$\frac{k_{1z}}{\varepsilon_1} + \frac{k_{mz}}{\varepsilon_m} = 0, \quad (15)$$

where  $\varepsilon_1$  is the permittivity of the dielectric, and  $\varepsilon_m$  is the permittivity of the metal. A surface plasmon is an evanescent mode of a system, and therefore does not propagate in the  $z$ -direction. This means that for each surface plasmon, the  $k_z$ -component of the wavevector is imaginary:

$$k_{nz} = \sqrt{k_n^2 - k_{nx}^2} = +i\sqrt{k_{nx}^2 - k_n^2}, \quad (16)$$

where  $n = 1, m$ , and  $k_{nx}^2 - k_n^2 > 0$ . The positive sign in front of the radical is required for the solutions of Eq. (12) to converge as  $|z| \rightarrow \infty$ . Given these conditions for Eq. (16), one can determine from Eq. (15) that the dielectric functions must satisfy

$$\varepsilon_1 \varepsilon_m < 0. \quad (17)$$

For real permittivities this condition is met only if one of the permittivities is negative, which is generally possible only for metallic materials. In other words, Eq. (17) states that surface plasmons exist on dielectric-metal interfaces.

A way to characterize surface plasmons is to identify them by the component of the wavevector that is parallel to the surface. The boundary conditions, Eq. (8), state that this component is constant at the interface. Using Eq. (15), and (16) and solving for  $k_x$  one can derive the surface plasmon dispersion relation relating  $k_x$  to the angular frequency  $\omega$  with:

$$k_x = \frac{\omega}{c} \sqrt{\frac{\varepsilon_1 \varepsilon_m}{\varepsilon_1 + \varepsilon_m}}, \quad (18)$$

where  $c$  is the speed of light. Figure 2.2.1 shows the surface plasmon dispersion relation for three different interfaces: Gallium nitride (GaN) - Ag, PVA (a clear plastic used to protect the samples) - Ag, and Air-Ag. Each plot contains also the light's line of each dielectric. The propagating modes of the the systems are towards the smaller  $k_x$ -values from the light line. The surface plasmon dispersion curve is located towards higher  $k_x$  values from light's dispersion curve. This reflects the fact that the surface plasmons are non-radiating solutions; i.e. they cannot escape the surface on their own. Interestingly the surface plasmon dispersion relation has an asymptotic limit for large  $k_x$ . The asymptotic frequency limits are determined by the plasma frequency of the metal and the dielectric function of the corresponding dielectric.

In more complex geometries the surface plasmon dispersion relation cannot be solved analytically, and thus a numerical solution is needed. As an example, a numerical solution for Eq. (15) is considered. Fig. 3 shows the left hand side of Eq. (15) as a function of  $\omega$  and  $k_x$ . The correspondence between the plots in Fig. 2.2.1 and 3 is clear. The dark blue areas in Fig. 3 are the solutions for the surface plasmon condition. Similar numerical method of identifying the zeros from a surface will be useful later when more complicated systems are considered.

### 2.2.2 Skin Depth

An important property of a surface plasmons is the skin depth. Since surface plasmons are evanescent waves bound to the surface, the skin depth is a description of how rapidly the electric field diminishes as a function of distance from the surface. It is defined as the inverse of  $k_z$  and can be calculated using Eq. (16):

$$l_n = \frac{1}{k_{nz}} = \frac{c}{\omega} \left( \frac{\varepsilon_1 + \varepsilon_m}{\varepsilon_{1,m}^2} \right)^{1/2}, \quad k_{nx} > k_n. \quad (19)$$

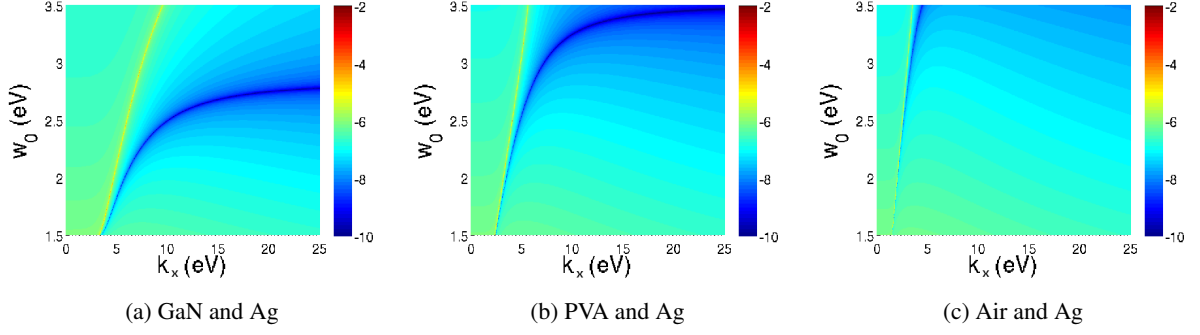


Figure 3: A numerical solution for the dispersion relation of surface plasmons. A plot of the left-hand side of Eq. (15), for which the zeros of the surface are to be interpreted as the dispersion relation for SPs. Note the similarity to Fig. 2.2.1

Skin depth is a specific property for each surface plasmon, and different in the two materials. For example, for a GaN-Ag surface plasmon, for energies varying from 1,5eV to 3,5eV, the skin depth is between 25 and 170 nm in the GaN, and 25 and 60 nm in the silver.

### 2.2.3 Surface Plasmons in Thin Films

In this subsection, the evanescent solutions to the wave equation in geometry of Fig. 4 is presented. The solution is again constructed from the planewave solutions in each material, and combined according to the boundary conditions. As noted in the previous section, only the TM-polarization is able to uphold surface plasmons, and thus only the TM-polarization is discussed here. The piecewise planewave solutions for each material layer read:

$$\begin{aligned} \mathbf{E}_1 &= \begin{pmatrix} E_{1x} \\ 0 \\ E_{1z} \end{pmatrix} e^{i(k_{1x}x - k_{1z}(z+a) - \omega t)} \\ \mathbf{H}_1 &= \begin{pmatrix} 0 \\ H_{1y} \\ 0 \end{pmatrix} e^{i(k_{1x}x - k_{1z}(z+a) - \omega t)} \end{aligned}, \quad z < -a, \quad (\text{dielectric 1}), \quad (20a)$$

$$\begin{aligned} \mathbf{E}_m &= \begin{pmatrix} E_{+mx} \\ 0 \\ E_{+mz} \end{pmatrix} e^{i(k_{mx}x + k_{mz}z - \omega t)} + \begin{pmatrix} E_{-mx} \\ 0 \\ E_{-mz} \end{pmatrix} e^{i(k_{mx}x - k_{mz}z - \omega t)} \\ \mathbf{H}_m &= \begin{pmatrix} 0 \\ H_{+my} \\ 0 \end{pmatrix} e^{i(k_{mx}x + k_{mz}z - \omega t)} + \begin{pmatrix} 0 \\ H_{-my} \\ 0 \end{pmatrix} e^{i(k_{mx}x - k_{mz}z - \omega t)} \end{aligned}, \quad -a < z < a, \quad (\text{metal}), \quad (20b)$$

$$\begin{aligned} \mathbf{E}_2 &= \begin{pmatrix} E_{2x} \\ 0 \\ E_{2z} \end{pmatrix} e^{i(k_{2x}x + k_{2z}(z-a) - \omega t)} \\ \mathbf{H}_2 &= \begin{pmatrix} 0 \\ H_{2y} \\ 0 \end{pmatrix} e^{i(k_{2x}x + k_{2z}(z-a) - \omega t)} \end{aligned}, \quad z > a, \quad (\text{dielectric 2}), \quad (20c)$$

where the indices are the same as in Fig. 4, and  $2a$  represents the thickness of the metal film. As before, the requirements set by the boundary conditions at each interface lead to a system of



Figure 4: A film of metal surrounded by semi-infinite dielectric layers. The metal is capable of supporting a surface plasmon on each interface. If the thickness of the film (2a) is on the order of the skin depth of the surface plasmons, the two plasmons can couple.

equations. Solving this system results in the following condition:

$$\frac{(1 + \frac{k_{1z}\epsilon_m}{k_{mz}\epsilon_1})(1 + \frac{k_{2z}\epsilon_m}{k_{mz}\epsilon_2})}{(1 - \frac{k_{1z}\epsilon_m}{k_{mz}\epsilon_1})(1 - \frac{k_{2z}\epsilon_m}{k_{mz}\epsilon_2})} - e^{2ik_md_m} = 0, \quad (21)$$

where  $d_m = 2a$  is the thickness of the metal. This equation is a generalization of the single interface surface plasmon condition, Eq. (15). The equation is so complex that a dispersion relation for the surface plasmons cannot be solved analytically. A simplification of the problem is to assume that the system is symmetric: this means that a silver layer is surrounded by the same material on both sides ( $\epsilon_1 = \epsilon_2 = \epsilon$ ). Eq. (21) then becomes

$$\left( \frac{\epsilon_m}{k_{mz} \tanh(\frac{k_{mz}d_m}{2})} + \frac{\epsilon}{k_z} \right) \left( \frac{\epsilon_m}{k_{mz} \coth(\frac{k_{mz}d_m}{2})} + \frac{\epsilon}{k_z} \right) = 0. \quad (22)$$

The form of this equation suggests that the surface plasmon dispersion splits into two separate solutions, one surface plasmon on each interface. Assuming that the metal is much thicker than the surface plasmon's skin depth in the given metal ( $a \gg l$ ), it trivially follows that the two surface plasmons exist independently of each other. When the the thickness is on the order of the skin depth, the situation becomes more complex. Fig. ?? shows a numerical solution of the left-hand side of Eq. (22), for semi-infinite GaN layers surrounding varying thicknesses of silver films. The figure shows how the surface plasmon dispersion relation splits into symmetric and antisymmetric solutions [?].

If the symmetry of the system is broken and the metal is surrounded by two different dielectrics, one must return to Eq. (21) to study the surface plasmons of the structure. Fig. ?? is a numerical solution of the left-hand side of Eq. (21), for a silver film of varying thickness, surrounded by a layer of PVA on one side, and GaN on the other. For thick metal layers the dispersion follows the dispersion relations of two separate interfaces between Ag and PVA and Ag and GaN. As the metal becomes thinner, the separation between the dispersion curves of the surface increases in a similar manner to the splitting seen in Fig. ??, as a result of the surface plasmons interacting. A more complete discussion on the subject may be found in [?].

### 2.3 The Effect of a Grating

Surface plasmons are bound modes of a structure and thus unable to leave the interface. However, there are few practical ways to couple a surface plasmon to the free optical modes of the surrounding materials. In the experiment studied in this thesis, the coupling is achieved by the use of a periodic grating. A periodic grating can shift the wavevector component parallel to the surface [?] as defined by the following equation:

$$k'_x = k_x + K = k_x \pm \frac{2\pi}{a}n, \quad n = 0, 1, 2, \dots \quad (23)$$

where  $k'_x$  is the modified wavevector,  $k_x$  the original wavevector component parallel to the surface,  $K = 2\pi/a$  is the grating wavevector,  $a$  is the grating period, and  $n$  the diffraction order in question.

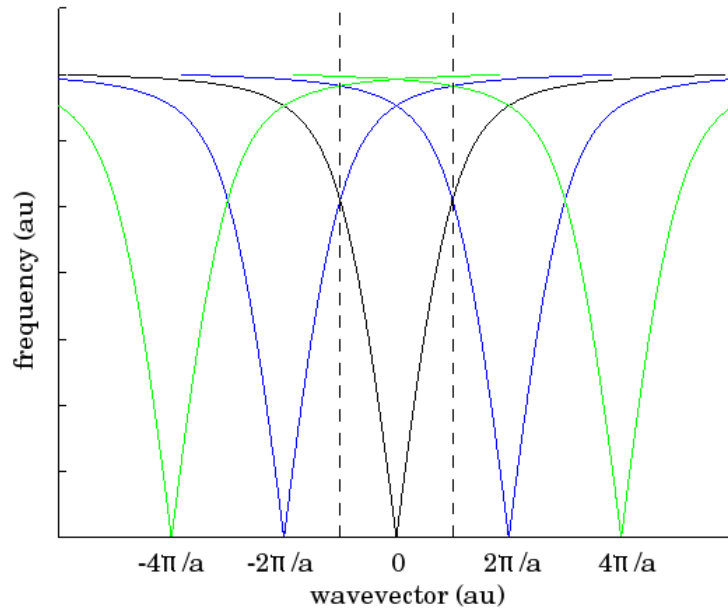


Figure 7: A periodic grating can influence the surface plasmon by shifting the folding the dispersion relation into the first Brillouin zone.

For surface plasmons, this scattering essentially shifts the surface plasmon dispersion relation by  $K$ . Fig. 7 shows the effect of multiple shifts of an SP dispersion relation in an arbitrary scale. The original function appears to 'fold' into the are specified by the dashed line. For this reason the effect seen is called folding.

### 3 Computational Methods

This section covers the computational tools used in this study regarding layered surfaces. First, the transfer matrix method [?] and the related theory is introduced. Then, the details of using the method are discussed.

#### 3.1 Transfer Matrix Method

The transfer matrix method (TMM) is a method for calculating the propagation of electromagnetic waves in layered structures. It uses the symmetry of a parallel planar structure relate the incoming and outgoing fields on one side of a structure to the fields on the other side. The transfer matrix method describes the relations of the piecewise solutions of the electric and magnetic fields in each layer of piecewise continuous material, in matrix form. The propagation within and between the layers are described by matrices, and the structure is combined to a single matrix that represents the system as a whole.

##### 3.1.1 Field Propagation and the Propagation Matrix

The propagation matrix describes the relationship of electromagnetic planewaves between two points in homogeneous material, as illustrated in Fig. 8.

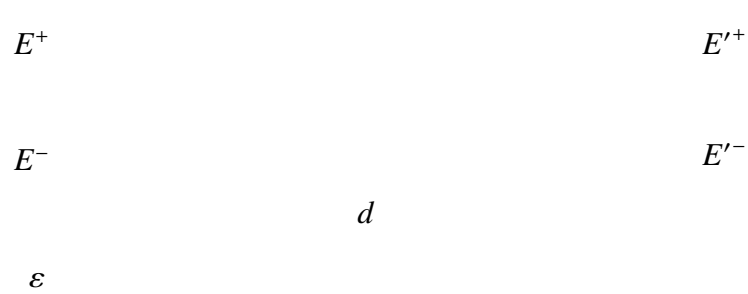
$$\begin{pmatrix} E^+ \\ E^- \end{pmatrix} = P \begin{pmatrix} E'^+ \\ E'^- \end{pmatrix} = \begin{bmatrix} e^{ik_x d} & 0 \\ 0 & e^{-ik_x d} \end{bmatrix} \begin{pmatrix} E'^+ \\ E'^- \end{pmatrix}$$


Figure 8: The propagation matrix is a solution of the Maxwell's equations for a propagating wave in a homogeneous material over a distance  $d$ .

The planewave solution [Eq. (4)] for a uniform non-magnetic media defines the solution so that a full knowledge of the field at a single point can be used to determine the field at any other point within the material. Referring to Fig. 8, let  $E^+$  and  $E^-$  represent the initial conditions for the field at a given point, for waves traveling in opposite directions. The field can then be compactly described by the propagation matrix  $P$  as

$$\begin{pmatrix} E^+ \\ E^- \end{pmatrix} = P \begin{pmatrix} E'^+ \\ E'^- \end{pmatrix}. \quad (24)$$

The choice of the source point is arbitrary, as long as full knowledge of the field is present. Thus, the previous example can be reversed:

$$\begin{pmatrix} E'^+ \\ E'^- \end{pmatrix} = P_- \begin{pmatrix} E^+ \\ E^- \end{pmatrix}, \quad (25)$$

where, index of  $P_{\pm}$  defines the location of the source in reference to the end point, as in Fig. 8, and determines the appropriate terms of the propagation matrix:

$$P_{\pm} = \begin{bmatrix} e^{\pm ik_x d} & 0 \\ 0 & e^{\mp ik_x d} \end{bmatrix}. \quad (26)$$

where the elements of the propagation matrix are composed of the propagation terms of the planewave solution.

### 3.1.2 Interface of Two Semi-Infinite Materials

At the interface of two materials the fields must satisfy the boundary conditions. The reflection and transmission at the interface is therefore described by the Fresnel coefficients of Section 2.1.2.

$$\begin{array}{cc} \epsilon_1 & \epsilon_2 \\ E_1^+ & E_2^+ \\ E_1^- & E_2^- \end{array}$$

Figure 9: The interface of two semi-infinite structures. The reflection and transmission of the fields are described by the Fresnel coefficients.

The input and the output fields,  $E_1^+, E_1^-, E_2^+, E_2^-$  are then related by the condition

$$\begin{pmatrix} E_1^- \\ E_2^+ \end{pmatrix} = \begin{bmatrix} r_+ & t_- \\ t_+ & r_- \end{bmatrix} \begin{pmatrix} E_1^+ \\ E_2^- \end{pmatrix} \quad (27)$$

where  $r$  and  $t$  are the Fresnel coefficients for the given polarizations as described by Eq. (9) and (10), and the subscripts  $+/-$  represent the direction of the incident wave for determining the coefficients. The fields can then be solved to give a solution of the form

$$\begin{pmatrix} E_1^+ \\ E_1^- \end{pmatrix} = \begin{bmatrix} \frac{1}{t_+} & \frac{-r_-}{t_+} \\ \frac{r_+}{t_+} & \frac{-r_+r_-+t_+t_-}{t_+} \end{bmatrix} \begin{pmatrix} E_2^+ \\ E_2^- \end{pmatrix}. \quad (28)$$

For the TE polarization the transfer matrix of a single interface can be written as

$$\begin{pmatrix} E_1^+ \\ E_1^- \end{pmatrix} = \frac{1}{2} \begin{bmatrix} (1 + \frac{k_{3z}}{k_{1z}}) & (1 - \frac{k_{3z}}{k_{1z}}) \\ (1 - \frac{k_{3z}}{k_{1z}}) & (1 + \frac{k_{3z}}{k_{1z}}) \end{bmatrix} \begin{pmatrix} E_2^+ \\ E_2^- \end{pmatrix} = M_{TE}^+ \begin{pmatrix} E_2^+ \\ E_2^- \end{pmatrix} \quad (29)$$

or

$$\begin{pmatrix} E_2^+ \\ E_2^- \end{pmatrix} = \frac{1}{2} \begin{bmatrix} (1 + \frac{k_{1z}}{k_{3z}}) & (1 - \frac{k_{1z}}{k_{3z}}) \\ (1 - \frac{k_{1z}}{k_{3z}}) & (1 + \frac{k_{1z}}{k_{3z}}) \end{bmatrix} \begin{pmatrix} E_1^+ \\ E_1^- \end{pmatrix} = M_{TE}^- \begin{pmatrix} E_1^+ \\ E_1^- \end{pmatrix}. \quad (30)$$

For TM polarization one similarly obtains

$$\begin{pmatrix} E_1^+ \\ E_1^- \end{pmatrix} = \frac{1}{2} \begin{bmatrix} (1 + \frac{k_{3z}\epsilon_1}{k_{1z}\epsilon_3}) & (1 - \frac{k_{3z}\epsilon_1}{k_{1z}\epsilon_3}) \\ (1 - \frac{k_{3z}\epsilon_1}{k_{1z}\epsilon_3}) & (1 + \frac{k_{3z}\epsilon_1}{k_{1z}\epsilon_3}) \end{bmatrix} \begin{pmatrix} E_2^+ \\ E_2^- \end{pmatrix} = M_{TM}^+ \begin{pmatrix} E_2^+ \\ E_2^- \end{pmatrix} \quad (31)$$

or

$$\begin{pmatrix} E_2^+ \\ E_2^- \end{pmatrix} = \frac{1}{2} \begin{bmatrix} (1 + \frac{k_{1z}\epsilon_3}{k_{3z}\epsilon_1}) & (1 - \frac{k_{1z}\epsilon_3}{k_{3z}\epsilon_1}) \\ (1 - \frac{k_{1z}\epsilon_3}{k_{3z}\epsilon_1}) & (1 + \frac{k_{1z}\epsilon_3}{k_{3z}\epsilon_1}) \end{bmatrix} \begin{pmatrix} E_1^+ \\ E_1^- \end{pmatrix} = M_{TM}^- \begin{pmatrix} E_1^+ \\ E_1^- \end{pmatrix}. \quad (32)$$

## 3.2 The General Form

The power of the transfer matrix method lies in the form of the matrix solutions allowing the description of complex piecewise continuous structures by chaining the propagation and interface matrices of single layers and interfaces. For example, the multilayer structure of Fig. 10 can simply be described by

$$\begin{pmatrix} E_n^+ \\ E_n^- \end{pmatrix} = M_{n,n-1} P_{n-1} M_{n-1,n-2} \dots M_{3,2} P_2 M_{2,1} \begin{pmatrix} E_1^+ \\ E_1^- \end{pmatrix} = M_{TOT} \begin{pmatrix} E_1^+ \\ E_1^- \end{pmatrix}, \quad (33)$$

where each  $P_n$  describes the propagation matrix of specific layer, and  $M_{ij}$  describes the interface matrix, where  $j$  points to the incident material and  $i$  to the transmitted material. Additionally, note that  $M_{TOT}$  is a two-by-two matrix that contains all information pertaining to wave propagation in the structure.

### 3.2.1 Reflectivity and Transmissivity

The formulation of the transfer matrix method simplifies the calculation of the optical properties of a complex system. For example, the reflection and transmission coefficients for optical power are defined for a system with an incident, reflected and transmitted fields [?], which in terms of the TMM is stated as

$$\begin{pmatrix} E_n^+ \\ E_n^- \end{pmatrix} = \begin{bmatrix} a & b \\ c & d \end{bmatrix} \begin{pmatrix} 0 \\ E_1^- \end{pmatrix} = M_{TOT} \begin{pmatrix} 0 \\ E_1^- \end{pmatrix}, \quad (34)$$

from which the reflection ( $R$ ) and transmission ( $T$ ) coefficients are obtained directly in terms of the matrix elements:



$$\begin{array}{ccccccc}
\varepsilon_1 & & \varepsilon_2 & & \varepsilon_3 & & \dots\dots\dots & & \varepsilon_{n-2} & & \varepsilon_{n-1} & & \varepsilon_n \\
\\
E_1^+ & E_2^+ & & E_2'^+ & E_3^+ & & E_3'^+ & & \dots\dots\dots & & E_{n-2}^+ & E_{n-2}'^+ & E_{n-1}^+ & & E_{n-1}'^+ & E_n^+ \\
E_1^- & E_2^- & & E_2'^- & E_3^- & & E_3'^- & & \dots\dots\dots & & E_{n-2}^- & E_{n-2}'^- & E_{n-1}^- & & E_{n-1}'^- & E_n^- \\
\\
P_2 & & P_3 & & \dots\dots\dots & & P_{n-2} & & P_{n-1} \\
\\
M_{2,1} & & M_{3,2} & & M_{4,3} & & \dots\dots\dots & & M_{n-2,n-3} & & M_{n-1,n-2} & & M_{n,n-1}
\end{array}$$

Figure 10: The transfer matrix for a given layered structure is constructed piece by piece from alternating the interface and the propagation matrices.  $M_{n,m}$  represents the interface matrix between layers n,m, and  $P_m$  represents the propagating matrix in layer m.

$$R = r^2 = \left( \frac{E_n^+}{E_n^-} \right)^2 \bigg|_{E_1^+=0} = \left( \frac{b}{d} \right)^2, \quad (35a)$$

$$T = t^2 = \left( \frac{E_1^-}{E_n^-} \right)^2 \bigg|_{E_1^+=0} = \left( \frac{1}{d} \right)^2. \quad (35b)$$

### 3.2.2 Electric Field Profile

The transfer matrix method can also be used to calculate the spatial distribution of the electric field of a specified structure [?]. If the forward and backward propagating fields are known at any position in the structure, the fields can then be calculated at any other point by the transfer matrix between the points. The unknowns of this approach are typically the initial field. Due to the linearity of the system, however one can separately set the transmitted fields to fixed values, e.g. set  $[E_2^+, E_2^-] = [C, 0]$  and propagate the field backwards to obtain the incident and reflected fields.

### 3.2.3 Bound Modes

The transfer matrix method does not take into consideration whether the solution it provides is physical (i.e. does the solution diverge) or not. It is simply a mathematical solution to a differential equation. The physically reasonable solutions of the system must be found, which poses some problems when working with complex structures. There are two possible options, the first being fully numerical one, as proposed by Chilwell [?]. This method is simple: The electric field profile is calculated, as explained in the previous section, for the system. This is repeated for any number of different wavevectors and frequencies. The aim is to search for the combinations for which the electric fields converge at the edges of the solution. These represent the bound modes of the system.

Another closely related option is to use the transfer matrix to find the physically relevant solutions.

The bound modes have the peculiar property that they can exist without an external stimuli, so that the condition

$$\begin{pmatrix} \mathbf{E}_2^+ \\ 0 \end{pmatrix} = \begin{bmatrix} a & b \\ c & d \end{bmatrix} \begin{pmatrix} 0 \\ \mathbf{E}_2^- \end{pmatrix}, \quad (36)$$

holds for non-zero  $E_2^+$  and  $E_2^-$ . This corresponds to the requirement

$$d = 0. \quad (37)$$

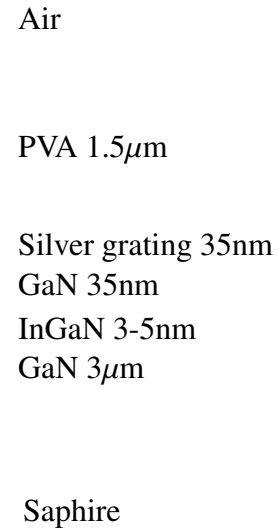
In cases where the planar system is simple, one can calculate  $d$  using the transfer matrix approach and analytically solve the dispersion relation from the condition of Eq. (37). In typical structures, one must solve the dispersion relations of the bound modes numerically, e.g. by searching for the zeros of the element  $d$  in the transfer matrix.

## 4 Simulation Results and the Experimental Setup

This section first reviews the experiment of our collaborators and the structure of the measured samples. The transfer matrix method is then applied to a planar version of the structure and selected aspects of the results are discussed and analyzed.

### 4.1 The Experimental Setup

Our collaborators measured the luminescence and reflectivity of sample structures consisting of semiconductor layers grown on a sapphire substrate, metal grating and a protective PVA resist layers as shown in Fig. 11. The main variables in the experiment were the layer thicknesses and the grating period of the silver, which was varied from 200nm to 400nm.



Air

PVA 1.5 $\mu$ m

Silver grating 35nm  
GaN 35nm  
InGaN 3-5nm  
GaN 3 $\mu$ m

Sapphire

Figure 11: Basic structure of the samples studied in the experiment.

The reflectivity was measured by shining collimated white light on the surface of the sample and guiding a Fourier transformed and spectrally decomposed reflected light on a CCD array so that the directional and spectral dependence of the reflection could be observed.

### 4.2 Modeled Structure

To obtain further insight into the reflection patterns observed, initial simulations are made with a simplified structure - shown in Fig. 12. In the simplified structure the InGaN quantum well is not present and the silver grating has been approximated as a solid silver layer.

The simplified structure does not contain a quantum well, and is therefore not suitable for simulating the luminescence of the samples. Nonetheless, it reasonably approximates the mode structure and the plasmon dispersion relations, and therefore can be used as a first approximation.

### 4.3 Analysis of the Structure

In what follows, the modeled structure is analyzed using the transfer matrix method as introduced in Section 3. First, the reflectivity of the modeled structure, as defined by Eq. (35), is calculated

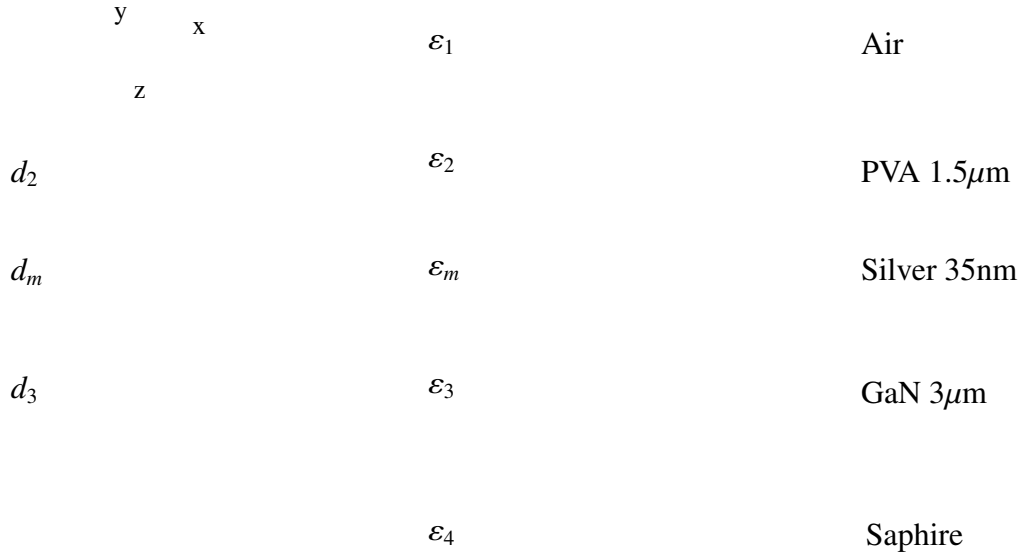


Figure 12: The simplified structure used to model the samples of the experiment. The silver grating has been approximated as homogeneous layer, and the quantum well has been removed.

and compared to the experimental results provided by our partners. Next, the bound modes of the modeled system are calculated. Finally, the effects of the silver grating are simulated by folding, as shown in Section 2.3.

#### 4.3.1 Reflectivity

The reflectivity of the sample structure can be calculated using the transfer matrix method and Eq. (35a). The result is shown in Fig. 13a as a function of wavelength and incidence angle. The reflection coefficient exhibits Fabry-Perot - type resonances for the two cavities formed by the PVA and the GaN layers. As a comparison Fig. 13b shows the corresponding experimental results of a reflectometry experiment. The image on the right has been scaled similar to the theoretical results, while the one in the middle has been zoomed to show the small interference patterns seen in the experiment

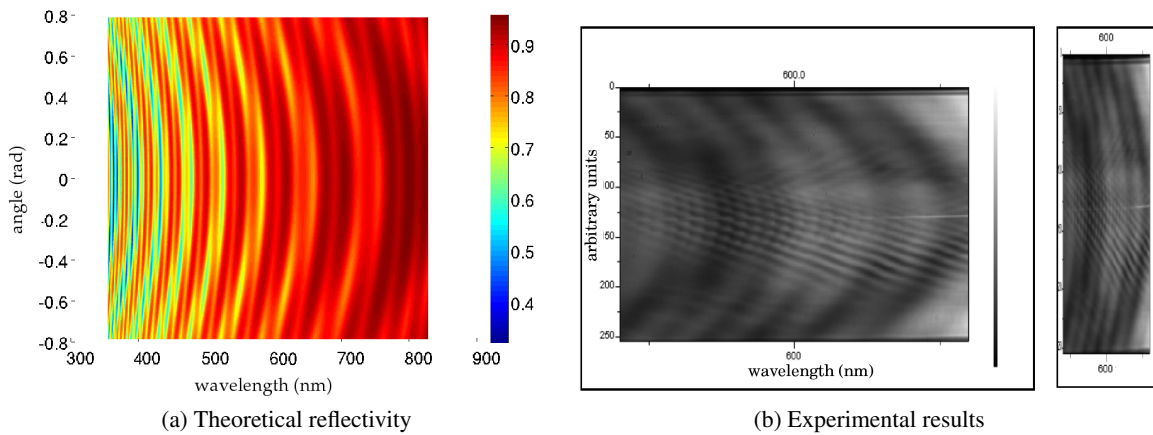


Figure 13: Reflectivity of the modeled structure is plotted in (a) Experimental results [?] for reflectivity are in (b), which contains two different horizontal scales for the same data. Note the similarities between the pictures: the large interference patterns are known to be caused by the Fabry-Perot cavities of the structure. The small interference pattern is only present in the experimental results.

The Fabry-Perot interferences of the PVA and GaN layers are present in both figures; the PVA layer is the source of the interference patterns with the largest period. The thicker GaN layer is the source of the shorter period modulation on the PVA interference pattern, and is also visible in all three images. The spatial layout of the Fabry-Perot interference patterns is quite similar in the modeled structure and the experimental results. This shows that the simple model is able to capture the salient features of the planar structures.

However, the smallest interference patterns seen in the experiment are not reproduced by the model. This is because the simple model only accounts for the modes of the system which are free to radiate in the air. Luckily, the phenomenological inclusion of the coupling of the bound and free space modes by the grating is relatively straightforward, as will be seen in the following sections.

#### 4.3.2 Bound Modes

The dispersion of the bound modes in the planar sample of Fig. 12 can be obtained by calculating the transfer matrix and requiring  $d = 0$  as described in Section 3.2.3. For the specific structure presented in Fig. 12, this condition can be expressed as

$$\frac{(1 - A \frac{k_{2z}\epsilon_m}{k_{mz}\epsilon_2})(1 - B \frac{k_{3z}\epsilon_m}{k_{mz}\epsilon_3})}{(1 + A \frac{k_{2z}\epsilon_m}{k_{mz}\epsilon_2})(1 + B \frac{k_{3z}\epsilon_m}{k_{mz}\epsilon_3})} - e^{2ik_m d_m} = 0, \quad (38)$$

where

$$A = \frac{e^{2ik_{2z}d_2} \frac{\frac{k_{2z}\epsilon_1}{k_{1z}\epsilon_2} - 1}{\frac{k_{2z}\epsilon_1}{k_{1z}\epsilon_2} + 1} - 1}{e^{2ik_{2z}d_2} \frac{\frac{k_{2z}\epsilon_1}{k_{1z}\epsilon_2} - 1}{\frac{k_{2z}\epsilon_1}{k_{1z}\epsilon_2} + 1} + 1}, \quad B = \frac{e^{2ik_{3z}d_3} \frac{\frac{k_{3z}\epsilon_1}{k_{4z}\epsilon_2} - 1}{\frac{k_{3z}\epsilon_1}{k_{4z}\epsilon_2} + 1} - 1}{e^{2ik_{3z}d_3} \frac{\frac{k_{3z}\epsilon_1}{k_{4z}\epsilon_2} - 1}{\frac{k_{3z}\epsilon_1}{k_{4z}\epsilon_2} + 1} + 1}. \quad (39)$$

Each index refers to the specific layer as defined in Fig. 12. This is a generalization of the thin-film model, specifically of the Eq. (20). To find the dispersion relation of the bound modes of the structure, the left hand side of Eq. (38) is plotted in Fig. 14. In the figure, the GaN-Ag and PVA-Ag surface plasmons are clearly visible. The red lines overlapping the surface plasmon are plots of the surface plasmon dispersion relation evaluated from Eq. (15), for respective surface plasmons. This shows that the locations of the surface plasmon's are only lightly shifted by the thin metal, as was the case with thin films in Section 2.2.3. The yellow lines represent light lines for air, PVA, GaN, from left to right. Between these lines, there are two new sets of patterns. The patterns between the PVA light line and the GaN light line are guided modes of the GaN layer, and similarly the patterns between the light line of air and the light line of PVA are the trapped modes of the PVA film.

Interestingly, the PVA-Ag surface plasmon's dispersion relation partly overlaps with the guided modes in the GaN. To gain an understanding of what is happening at such bound modes, let's take a look at the electric field profile of the modeled structure, using the method explained in Section 3.2.2. Fig. 15 shows the electric field profile of the bound modes for  $k_0 = 2.58$  eV, and for the  $k_x$  that correspond to the bound modes when  $4 \text{ eV} < k_x < 15 \text{ eV}$ . The figure contains a scaled electric field profile for the selected bound modes in sapphire, GaN, silver and PVA layers. The electric field profile for a GaN-Ag surface plasmon is shown at the top as an evanescent field, distinctly colored in red. With decreasing  $k_x$ , each bound mode below the surface plasmon mode represents an electromagnetic field that propagates dominantly in the GaN layer. This field undergoes a total internal reflection at the sapphire and PVA interfaces. These modes are trapped modes of the GaN layer.

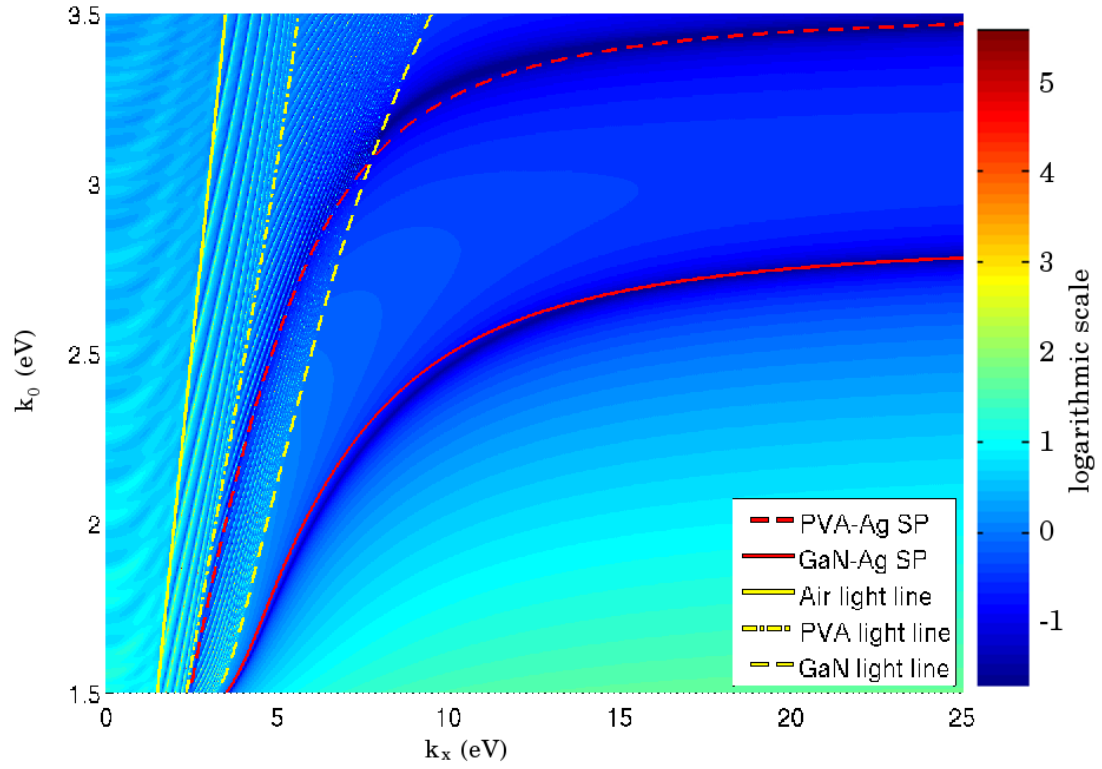


Figure 14: Numerical calculation for the bound modes of the modeled structure shown in Fig. 12. In addition to the two surface plasmonic curves, new pattern is present on the left hand side of the figure. The yellow dotted lines represent light lines air, PVA, GaN. Note how the PVA-Ag (the upper) surface plasmon is partially mixed in with the new pattern on the left hand side of the figure.

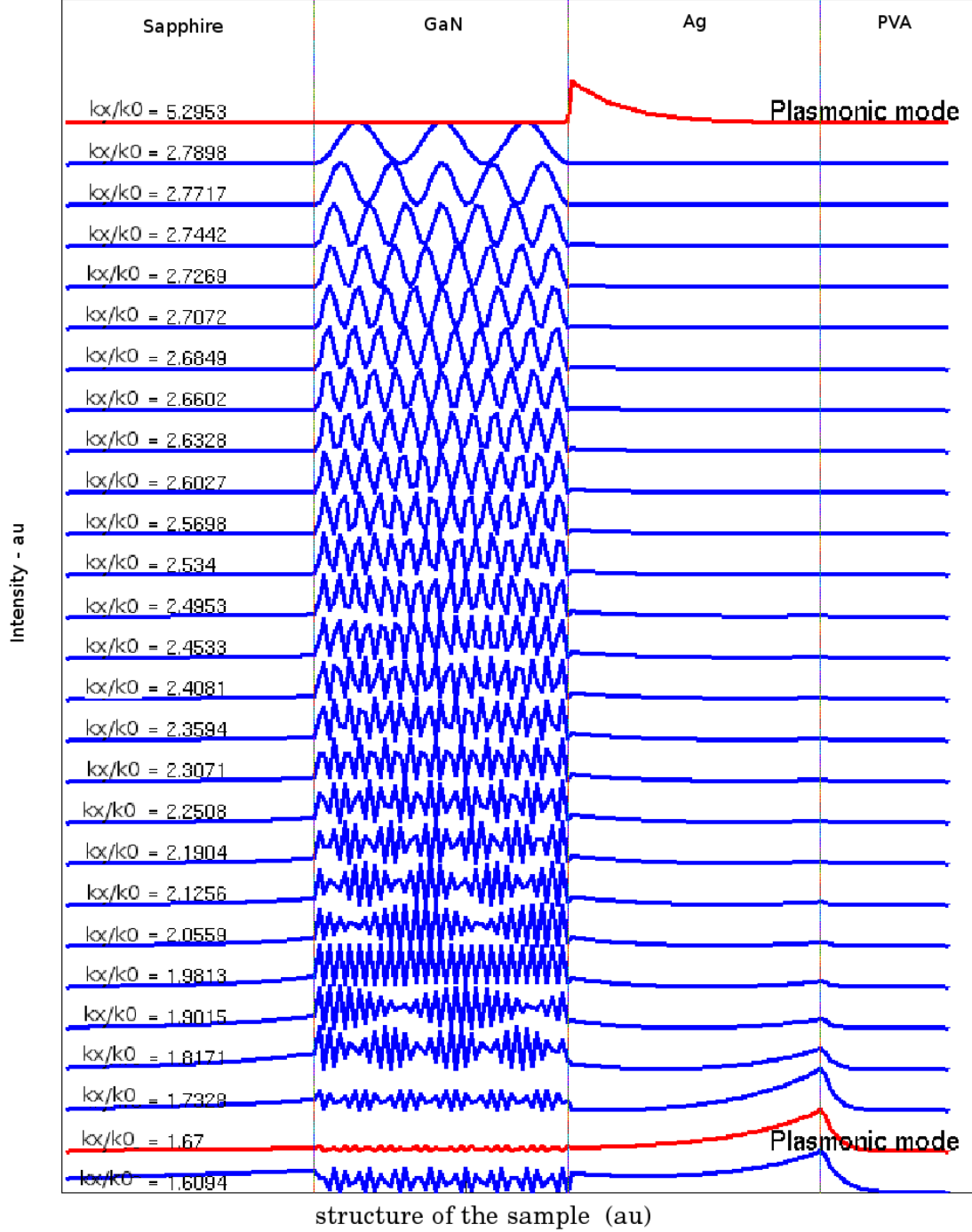


Figure 15: The electric field profile of the structure along the position  $k_0 = 2.58$  eV for the guided modes. The plasmon at the PVA-Ag metal interface couples with the guided modes of the GaN, which is seen in the electric field profiles as a non-zero electric field both in the GaN.

The red line at the bottom of Fig. 15 corresponds to the location of the PVA-Ag surface plasmon. It has the evanescent shape of a surface plasmon at the PVA-Ag interface, but it also exhibits a contribution extending to the GaN layer. The same characteristic is further seen in the electric field profiles above and below the lower frequency plasmonic mode. While these modes are not purely plasmonic, they do possess a plasmonic feature in the decaying wave at the PVA-Ag interface. This suggests that the PVA-Ag surface plasmon and the trapped fields in the GaN layer interact, forming

modes that are neither fully plasmonic nor trapped.

Similar analysis done for  $k_x$  at lower values ( $0 \text{ eV} < k_x < 4 \text{ eV}$ ) indicates that the pattern in Fig. 14 situated between the air and PVA light line is caused by the modes that are able to radiate in PVA, but go through total internal reflection on the PVA-air interface. Such fields are only partially reflected by the silver, and are transmitted through into GaN and sapphire in considerable amounts. Thus these fields are leaky modes of the system. Further characterization of their properties with the current model is out of scope of this work.

### 4.3.3 Effects of the Grating

The modeled structure does not take into consideration the grated form of the silver. To account for the grating, folding of the wavevector can be used to approximate its effects, as discussed in Section 2.3. This has been done in Fig. 16, where the  $k_x$  of data shown in Fig. 14 has been folded over a period of 310 nm and multiplied back into the original data. Additionally the axis have been flipped. The multiplication should retain the locations of the zeroes, or the bound modes of the system. Therefore this method will not produce accurate data, but it will give us the approximate locations for bound modes. For this reason scale of the figure is arbitrary.

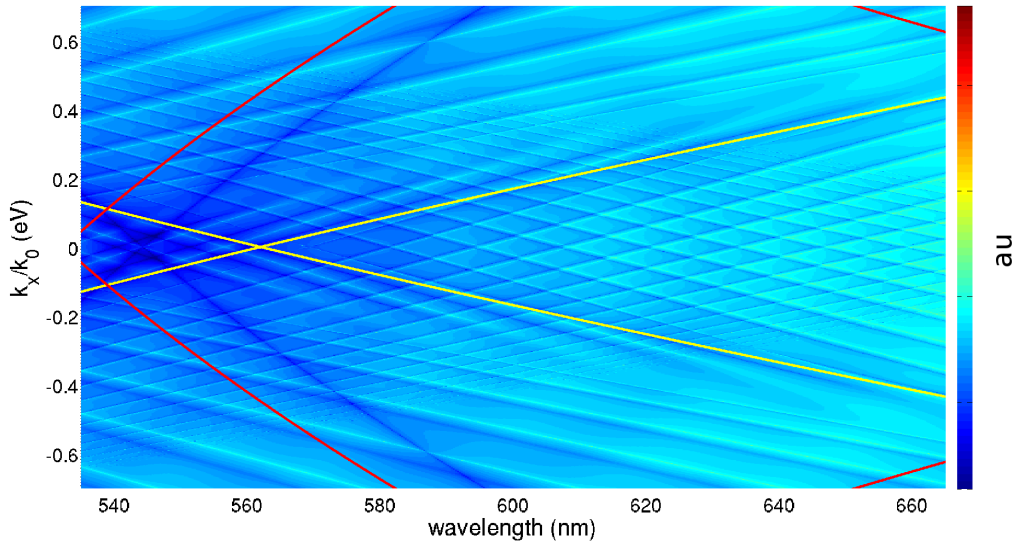


Figure 16: Mode structure of the simulated sample folded by a grating with a period 310nm. The web-like pattern on the right side of the figure is caused by the guided modes of the GaN layer. The yellow line is the PVA-Ag and the red line is the GaN-Ag surface plasmon dispersion relation of semi-infinite structure.

The yellow and red lines of 16 represent the folded PVA-Ag and GaN-Ag surface plasmon dispersion relations as obtained from Eq. (15), respectively. The darkest blue line is the location for the GaN-Ag surface plasmon as predicted by Eq. (38). Notice the shift it has undergone due to the thin layer of silver. The lighter blue lines present in the figure are the bound modes of GaN and PVA layers. These lines are similar to the unidentified pattern seen in the experimental results in Fig. 13b.

The specific period of 310 nm was chosen to compare the results of the theory with data from the reflectometry experiment, shown in Fig. 17. To ease the of comparison of the two figures, the axis of Fig. 16 have been confined to ranges visible in the experimental results. When comparing the two figures, it is very important to remember that the theoretical method used only predicts the location of the bound modes of the structure, not the strength of the fields.



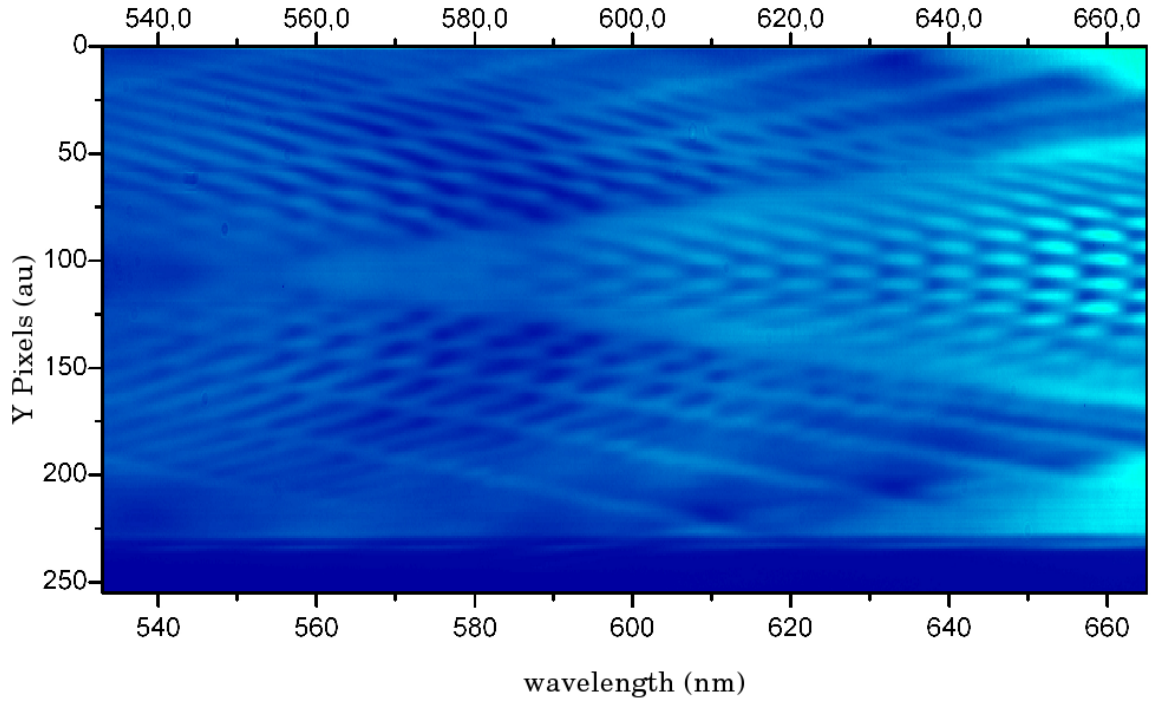


Figure 17: Data from the experiment [?], measuring the reflectivity of a sample with a grating periodicity of 310nm.

The similarities between the theoretical results and the reflectometry data strongly indicate that the source of the interference pattern observed in the experiment is the bounds modes of the GaN and PVA layer. These modes are coupled to the freely radiating modes of the air by the silver grating. To reiterate, the web-like pattern seen on the right hand side of the figures is caused by the trapped modes of the GaN layer, while the leaky modes of the PVA layer are the lines on the top and bottom with more space in between them. Similar effects have been reported in GaN waveguides with periodic photonic crystals [?].

The experimental results in Fig. 17 do not contain any trace of these surface plasmons. Considering how the PVA-Ag surface plasmons mixes with the GaN trapped modes, it may not be surprising that the surface plasmon itself seems to disappear. However, the disappearance of the GaN-Ag plasmon suggests that the plasmonic modes may experience large losses that make them practically invisible. This problem is however beyond the scope of this study.

## 5 Conclusions

This thesis started with theoretical review of the basic electromagnetic properties of matter, an introduction to surface plasmons in simple structures, and a short discussion on the effects of a grating on the electromagnetic fields of a structure. Next, the transfer matrix method (TMM) was presented and used to stimulate an experimental reflectometry setup used by our collaborators. The results accurately reproduced the interference patterns observed in the experiment and made it possible to identify the physical origin of the patterns.

The original aim of the experiment was to determine the coupling of surface plasmons to the quantum well and the free optical modes. However, instead of the expected plasmonic patterns, only interference patterns of unconfirmed origin were observed in the experiment. The results presented in this thesis allow identifying the source of the interference patterns as originating from the guided modes of the GaN layer and the leaky modes of the PVA layer. The disappearance of the plasmonic modes still remains at least partly unresolved. It is possibly related to the losses experienced by the plasmonic modes preventing efficient scattering of the plasmonic modes from the grating.

Future work regarding the continuation of this project should begin in finding a more quantitative method of accounting for the silver grating in the model. One possibility is to model the silver grating as a dielectric layer with a specific dielectric constant, as explained by Shen [?]. This will likely provide accurate results for the effects of the grating. An other option is to use Green's functions to solve the Maxwell's equations for a nano-scale metal grid, as shown by Vidal [?]. Additionally the Green's functions formalism could be used to model the luminescence from the quantum well. It would also be useful to implement a finite-element based numerical model for solving the Maxwell's equations in the given structures.

## Appendix - Material Properties

It is assumed that all the materials, metals and dielectrics, are non-magnetic and isotropic. The materials do not react to magnetic fields, and each dielectric function is only a function of frequency:

$$\mu_i = \mu_0 = 4\pi \times 10^{-7} \frac{N}{A^2} \quad (40)$$

$$\varepsilon = \varepsilon(\omega) \quad (41)$$

All dielectrics are assumed to be non-lossy. Thus the permittivity of any dielectric will only have a real part:  $\text{Im}(\varepsilon_{\text{dielectric}}) = 0$ . Below is a table containing the dielectric functions for all the dielectrics used in this report.

$\varepsilon_{air}$	1
$\varepsilon_{pva}$	$(1.511 + 46399 \frac{1}{\lambda^2} - 4.32127 \times 10^9 \frac{1}{\lambda^4})^2$
$\varepsilon_{gan}$	$(23.6837 - 0.176\lambda + 5.87178 \times 10^{-4}\lambda^2 - 9.84899 \times 10^{-7}\lambda^3 + 8.27566 \times 10^{-10}\lambda^4 - 2.78123 \times 10^{-13}\lambda^5)^2$
$\varepsilon_{saph}$	2.8900

where  $\lambda$  is the wavelength in nanometers. The PVA's permittivity was measured by our collaborators,

For the silver, a Drude model fit is used with following parameters [?] :

$w_p$	$1.3734 \times 10^{16}$
$w_T$	$1.32284 \times 10^{13}$
$\varepsilon_\infty$	4